

<https://doi.org/10.1038/s41545-024-00335-4>

Lifetime optimisation of integrated thermally and electrically driven solar desalination plants

Check for updates

Benedict Winchester^{1,2,3}, Gan Huang^{1,4}, Hamish Beath^{1,2,3}, Philip Sandwell^{1,2,3}, Jiajun Cen^{5,6}, Jenny Nelson³ & Christos N. Markides¹ ✉

We compare the performance of photovoltaic (PV), flat-plate and evacuated-tube solar-thermal (ST), and hybrid photovoltaic-thermal (PV-T) collectors to meet the energy demands of multi-effect distillation (MED) desalination plants across four locations. We consider three scales: 1700 m³day⁻¹, 120 m³day⁻¹ and 3 m³day⁻¹. We find a strong dependence of the capacity and configuration of the solar collectors on both the cost of sourcing electricity from the grid and the specific collector employed. We find specific costs as low as 7.8, 3.4 and 3.7 USDm⁻³ for the three plant capacities. We find that solar-driven systems optimised for the lowest specific cost result in CO₂eq emissions equal to, or higher than, those from grid-driven reverse osmosis (RO) and in line with PV-RO. This highlights the need to consider the environmental footprint of these systems to ensure that desalination is in line with the United Nations' Sustainable Development Goal 6.

As of 2018, the United Nations Children's Fund (UNICEF) estimates that one in three people globally are without access to clean water¹ whilst the number without access to electricity remains high at an estimated 745 million² having increased in 2022³. At the same time, the demands for power^{4–6} and clean water^{7,8} have continued to increase globally, both as populations rise^{7,9–11} and also as lower-income countries develop economically¹² and increase their standards of living^{13–15}; current freshwater withdrawals range by a factor of over 60 between low-income and high-income countries, from 20.9 litres/capita-day in the Democratic Republic of the Congo to over 1340 litres/capita-day in the United States of America as of 2020¹⁶. Desalination, the process of converting saline water into potable water¹⁷, currently accounts for around 0.6% of global greenhouse gas emissions¹⁸ with only about 1% of desalination currently powered by renewable energy¹⁹. Estimates put the energy-associated emissions of an MED desalination plant in the UAE operating for a 30 year lifetime at over 90% of the total lifetime emissions of the plant²⁰. With the demand for desalination set to rise by 40–50% by 2050¹¹, novel technologies need to be assessed and deployed to communities which currently lack a reliable source of clean drinking water in line with Sustainable Development Goal (SDG) 6, “clean water and sanitation for all”²¹.

Hybrid PV-T solar panels produce both electricity and heat from the same collector²². The most-common PV-T collectors tend to be thermally-

coupled—with the photovoltaic (PV) modules in direct thermal contact with the solar-thermal (ST) absorber material—and non-concentrating flat-plate collectors, due to the risk of damage to the PV cells^{23,24} and this being the easiest design to manufacture²⁵. As many desalination technologies require both electricity and heat, the ability to extract both of these from a single collector can provide potential synergistic benefits over stand-alone collectors^{26,27}.

As of 2020, 20% of renewable-energy-powered desalination was thermally driven: the main process being driven by heat²⁸. Whilst some membrane-based technologies—the other main desalination technique—utilise heat in some way^{29,30}, thermally driven technologies, which usually need both electricity and heat, present the greatest potential for integrations which utilise the efficiency benefits associated with PV-T collectors³¹.

Reverse osmosis (RO), an electrically-driven membrane-based process, accounted for 69% of desalination plants globally as of 2019^{32,33}. Although heated feedwater brings some performance benefits to RO (around a 3% increase in freshwater production per degree) it leads to faster rates of membrane degradation^{34,35}. Multi-stage flash (MSF) desalination is the second most widely used desalination technology. Accounting for 18% of installed plants as of 2019³², MSF plants are usually large in scale, supplying 50,000–70,000 tonnes of water per day³⁶—the drinking needs of up to 1.4 million people³⁷. MSF plants have issues surrounding corrosion, large capital investments, and maintenance in rural environments³⁸.

¹Clean Energy Processes (CEP) Laboratory, Department of Chemical Engineering, Imperial College London, London, UK. ²Grantham Institute – Climate Change and the Environment, Imperial College London, London, UK. ³Department of Physics, Imperial College London, London, UK. ⁴Institute of Microstructure Technology, Karlsruhe Institute of Technology, Karlsruhe, Germany. ⁵Department of Chemical Engineering, Imperial College London, London, UK. ⁶Desolenator BV, Maastricht, Netherlands. ✉e-mail: c.markides@imperial.ac.uk

MED desalination is the third most widely installed technology worldwide, with just under half as many plants installed as compared with MSF³². Needing both electricity and heat lends MED well to utilising PV-T collectors³⁹. Further, the lower electrical^{40,41} and thermal^{29,41} energy requirements of MED, combined with lower embedded emissions⁴², allows for higher-efficiency plant installations than for MSF. The lower operating temperatures of MED plants reduces the risk of scaling compared to MSF⁴³, whilst the possibility for smaller installations⁴⁴ lends MED well to community-scale contexts where access to clean drinking water⁴⁵ and electricity are lower⁴⁶.

Small-scale standalone systems of PV-T collectors, in combination with well-established ST and PV collectors, have the potential of addressing rural clean-water and electricity-access needs to help meet the goals of SDGs 6 and 7, “access to affordable, reliable, sustainable and modern energy for all,” whilst minimising carbon emissions in line with SDG 13, “urgent action to combat climate change and its impacts.” Thus far in the literature, the majority of PV-T-powered MED installations tend to consider only a single technology for energy generation, either concentrating^{47,48} (the majority of systems²⁷) or non-concentrating PV-T collectors⁴⁹. Further, there exists a gap in the range of existing open-source and licensable modelling tools available to assess PV-T-driven desalination systems, with most tools either considering only a single technology^{50,51} or having no scope for desalination and drinking-water demands^{52,53}. There is hence a need to develop a reliable methodology for assessing the performance of various renewable technologies, including PV-T collectors alongside more commonplace standalone PV and ST systems, for desalination.

This paper aims to present an open-source modelling tool for optimising the configuration of photovoltaic (PV), photovoltaic-thermal (PV-T) and solar-thermal (ST) collectors, along with battery storage and a grid connection, for powering an MED desalination plant. In this work, we apply this framework to three case-study MED plants to assess whether PV-T collectors are a cost-effective means of producing drinking water at three different scales when compared against the industry-standard of PV and grid-powered RO desalination^{32,33}, across four different case-study locations. By doing so, this paper aims to assess whether PV-T collectors can be cost-effective over the lifetime of a desalination plant for producing clean drinking water. We find a strong dependence between the choice of technology and specific collector and the overall cost of systems, and a strong correlation between the cost of grid electricity and the fraction of the plant’s power which was generated thermally. In the Methods, we outline the technologies considered, namely PV-T collectors and MED desalination.

Results and discussion

We undertook optimisations of the number of PV, PV-T and ST collectors, as well as the number of batteries, mass-flow rate through the collectors, and the size of the hot-water buffer tank installed. The optimisation process described in the Methods resulted in no optimisation of the buffer-tank capacity, potentially due to the slow-varying dependence of the total lifetime cost of the system on the tank capacity. We therefore fixed the capacity of the buffer tanks in our optimisation based on their mass-flow rate and the hourly water requirements of each plant modelled.

Optimisation for the lowest total lifetime cost

The storage-, solar- and grid-electricity fractions correspond to the fraction of the MED plant’s electricity demands that were met using energy supplied from battery storage, sourced directly from solar PV or PV-T collectors, or taken from the grid respectively. The auxiliary heating fraction is the fraction of the plant’s thermal requirements that were met using the auxiliary electrically-driven heat pump. This fraction can be negative, implying an excess of solar energy, and range up to one, which implies that all heating demand was met using the auxiliary heat pump. These fractions, for each location, are shown in Fig. 1 for 212 optimisations. The results are aggregated over the three plant capacities, the specifics of which are detailed in Table 3, and over the various technologies, which are detailed in the Supplementary Methods.

The data show a high sensitivity of the lowest-cost system on location which we attribute to variations in grid price. Abu Dhabi has a grid cost of 0.078 USDkWh_{el}⁻¹ (<https://www.addc.ae/en-US/business/Pages/RatesAndTariffs2018.aspx>) with plants, on average, using the grid to meet 38% of their electricity demands (26%–59% across the plants modelled), with electricity storage meeting 24%. Gando has a reduced reliance on the grid for night-time electricity. We attribute this to the price of grid electricity (0.146 USDkWh_{el}⁻¹⁵⁴) being more comparable to investing in electrical storage over the lifetime of the plant.

Tijuana and La Paz have specific grid costs over 35 times that of Abu Dhabi. As a result, plants in Tijuana and La Paz use electricity from the grid to meet 1.5% and 7.7% of their electricity demands respectively. These systems rely instead on battery storage (56% and 48% respectively), with the majority of grid-reliance visible in Fig. 1 reflecting data for the largest-scale plant, with grid fractions of 4.3% and 21% for Tijuana and La Paz respectively. We attribute this shift from grid-reliant systems towards self-reliant, solar-and-storage powered systems to the comparatively expensive cost of grid electricity in Mexico. We also attribute the increasing solar-electricity fraction across the four case-study locations to the rising mean cost of grid electricity. Solar electricity, sourced from either PV or PV-T collectors, meets 38%, 41%, 43% and 44% of the electrical demands of the plants in Abu Dhabi, Gran Carnaia, Tijuana and La Paz in Mexico respectively.

The increasing mean cost of grid electricity across the four case-study locations is also correlated with lower auxiliary-heating fractions, suggesting a shift towards systems which are more reliant on PV-T and ST collectors for hot-water heating than auxiliary electrically-driven heat-pump heating, powered through either the grid and PV panels. The mean number of collectors and batteries installed in each of the locations is given in Table 1.

Overall, there is a strong dependence of the grid-reliance of the systems on the cost of grid-sourced electricity: Abu Dhabi, with a cost of grid electricity of 0.078 USDkWh_{el}⁻¹, relied on grid-sourced power to meet 38% of the demands of the plant. This compares with Tijuana and La Paz, locations with a cost of grid electricity upwards of 2.91 USDkWh_{el}⁻¹, which relied on grid-sourced power to meet 1.5–7.7% of their demands on average. Between these two locations, there was also an observable shift in the reliance on battery storage for night-time power supply and ST and PV-T collectors for thermally driven heating.

We find that off-grid MED systems—plants powered wholly through solar collectors with electrical and thermal storage—are more affordable than grid-driven MED systems across all three case-study plants considered in three of our case-study locations, with grid-reliant systems only lower in cost for the smallest-scale⁵⁵ plant in Abu Dhabi, UAE, where the price of grid electricity was the lowest considered at 0.078 USDkWh_{el}⁻¹. However, due to the high emissions associated with electricity in the UAE, we conclude that this is not in line with the United Nations Sustainable Development Goal 6, “clean water and sanitation for all”²¹.

The optimum number of components installed for the largest-scale desalination plant considered are shown in Fig. 2. The results show both an overall trend—that an increasing cost of grid electricity results in larger systems—and transitions which occur between electrical, grid-reliant systems and thermally driven, off-grid systems. More analysis is given in the Supplementary Discussion.

The specific costs of desalinated water produced by the lowest-cost energy-supply system are shown in Fig. 3. The reference cost of a grid-powered RO system is shown as a hatched grey area, where the costs of grid electricity are taken from Tables 8 and 9 and the specific energy consumption of RO is taken as a range from 2–7 kWh_{em}⁻³⁵⁶. The reference cost of a PV-and-battery RO system is shown using a yellow hatched area. The specific cost of the energy-generation system was optimised for. This includes solar collectors, electrical and hot-water storage tanks, auxiliary heat pumps, water pumps and inverters. The other total expenditure costs—including the costs of labour, plant maintenance, and chemicals for pre-treatment of feedwater—are included in the results presented in Fig. 3.

The data show that, across the four case-study locations, the medium-scale desalination plant considered⁵⁷ afforded the lowest specific cost of

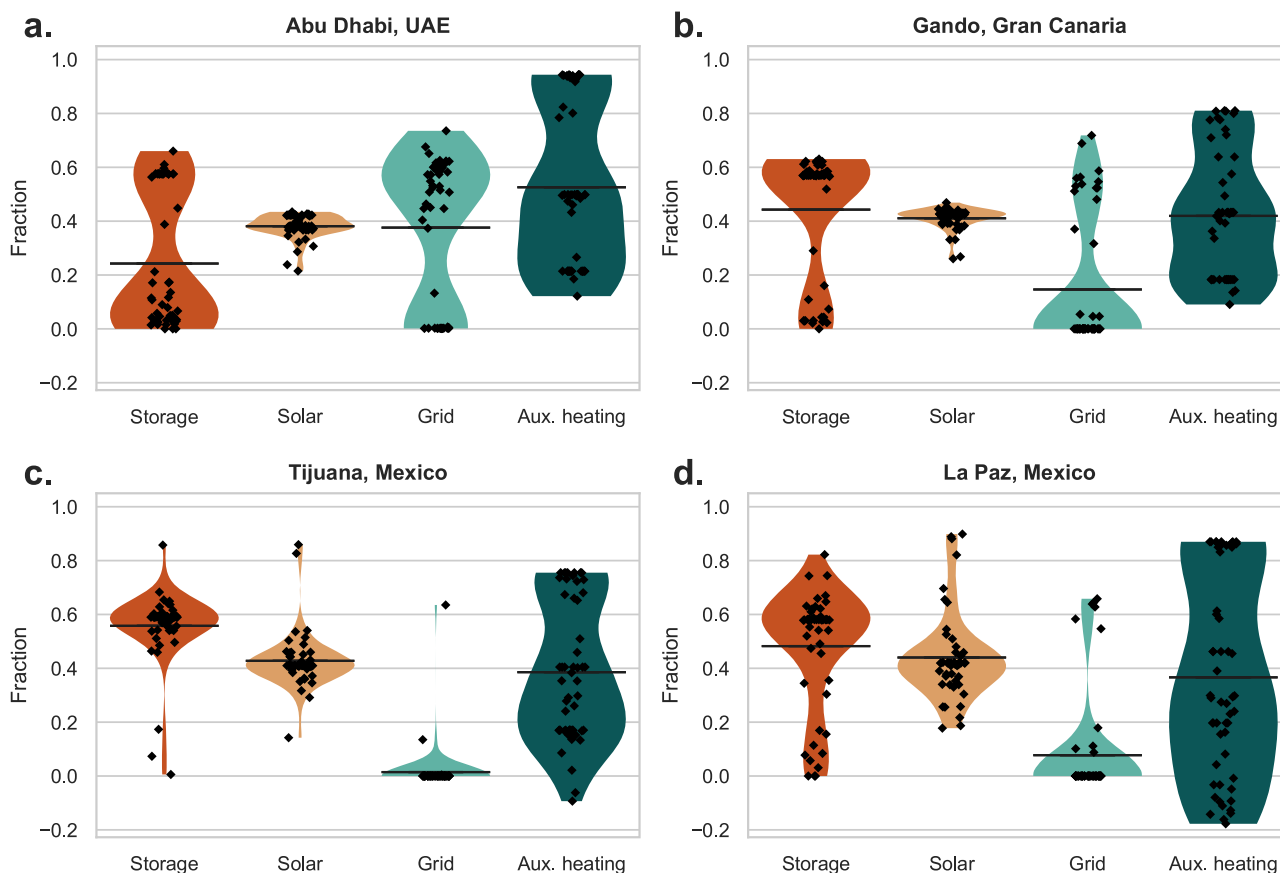


Fig. 1 | Storage, solar and grid fractions of electricity consumed. Scatter plot with an overlaid kernel-density estimate (KDE) in the form of a violin plot showing the storage, solar and grid electricity, and auxiliary-heating, fractions of the optimum system for 212 optimisations (resulting from different component types and plant sizes) for the lowest lifetime cost. The mean value is marked with a horizontal line.

The results are aggregated over the three MED plant sizes considered, as well as the various collector technologies, across the four case-study locations considered: (a) Abu Dhabi, UAE, (b) Gando, Gran Canaria, (c) Tijuana, Mexico and (d) La Paz, Mexico. The locations are listed in order of increasing mean grid electricity cost.

clean-water generation, with values of 3.4, 3.8, 4.0 and 3.6 USDm⁻³ for Abu Dhabi, Gando, Tijuana and La Paz respectively. This was followed by the largest-scale plant⁵⁸, with values of 3.7, 4.0, 4.3 and 3.9 USDm⁻³ respectively across the four locations, and by the smallest-scale plant considered⁵⁵, with values of 8.2, 8.1, 8.7 and 7.8 USDm⁻³ across the four locations respectively. These values are in line with those reported in the literature⁵⁹⁻⁶¹. Note that these values include those for the energy-generation system as well as the capital and operation and maintenance costs for the plants. Not included in Fig. 3 are the uncertainties deriving from the heat-pump model, around 6%⁶², or the weather data used, which can vary between 16%–38% for online tools that utilise the same data employed⁶³.

We attribute the fact that the medium-scale plant produces clean water with the lowest specific cost of the MED plants considered as being due to it having the lowest specific heat consumption of the three plants considered: 143 kWh_{th}m⁻³ as opposed to 153 kWh_{th}m⁻³ and 308 kWh_{th}m⁻³ for the largest- and smallest-scale plants considered respectively. Whilst the capital and operational costs scale with the capacity of the MED plants installed, following an economy-of-scale trend, these energy-system-related costs are primarily driven by specific heat consumption, which, in turn, is due to the design of each of the three plants considered. MED plants with a higher output of distilled water have an optimum number of effects, which is not necessarily correlated with the thermal requirements of the plant^{60,64}: MED plants with a greater number of effects require less thermal energy per unit water produced due to the smaller temperature drop across each effect. This reduction in the temperature drop per effect, however, results in a lower rate of freshwater production⁶⁴, meaning that plants which have a greater number of effects likely produce water less rapidly but more efficiently. This is visible in the number of effects for each of the plants considered: 3, 18, and 5^{55,57,58}.

The cost of grid-driven RO, shown as a grey-hatched area in Fig. 3, depends solely on the cost of grid-sourced electricity. In Abu Dhabi and Gando, where the grid costs 0.078 and 0.146 USDkWh_{el}⁻¹ respectively, grid-driven RO produces water with a lower specific cost than both PV-powered RO (PV-RO) and MED desalination. In Tijuana and La Paz, the higher grid cost results in both MED and PV-RO producing clean water with a lower specific cost.

The low grid-electricity fractions (visible in the teal bars) across all four locations in Fig. 3 demonstrate that an optimal choice of technology results in self-reliant systems other than for the smallest-scale plant in Abu Dhabi. We attribute the variations in the costs associated with the auxiliary heat pumps and solar inverters as being due to variations in the reliance between thermal and electrical heating: installations which rely more heavily on PV collectors and a grid connection for energy will have larger heat pumps; larger PV and PV-T arrays will result in larger inverter sizes.

Overall, the results show that the thermally driven MED plants considered were more affordable than grid-driven reverse osmosis (RO) within error in Tijuana and La Paz, Mexico, where the cost of grid-sourced electricity was greatest. In Abu Dhabi, UAE, and Gando, Gran Canaria, we found that grid-driven RO was more affordable than both PV-driven RO and the MED plants modelled due to the comparatively low cost of grid-sourced electricity. However, other factors, such as the salinity of the input water used, may mean that, despite this, RO is not the best choice in these locations.

The effect of changing which specific collector was included in the model on the total cost of the smallest plant—capable of producing 3 m³day⁻¹ of fresh water⁵⁵—is shown in Fig. 4. The choice of collectors which resulted in the lowest overall system cost for each plant size and location is

Table 1 | Mean number of PV, PV-T and ST collectors installed, aggregated over technology, for each of the case-study plants and locations considered determined by an optimisation to reduce the total lifetime cost of the system

Plant	$\dot{m}_{prod} / m^3 day^{-1}$	Location	Batteries	PV collectors	PV-T collectors	ST collectors
Small	3 ⁵⁵	Abu Dhabi	17	127	0	5
		Gran Canaria	108	227	5	9
		Tijuana	299	504	130	84
		La Paz	114	389	44	339
Medium	120 ⁵⁷	Abu Dhabi	3000	2810	4	70
		Gran Canaria	4920	3800	83	566
		Tijuana	5580	5840	45	1420
		La Paz	5110	3210	727	233
Large	1694 ⁵⁸	Abu Dhabi	43600	42000	213	1860
		Gran Canaria	74100	57900	4870	4730
		Tijuana	69800	69600	18000	28300
		La Paz	46400	35300	14400	39300

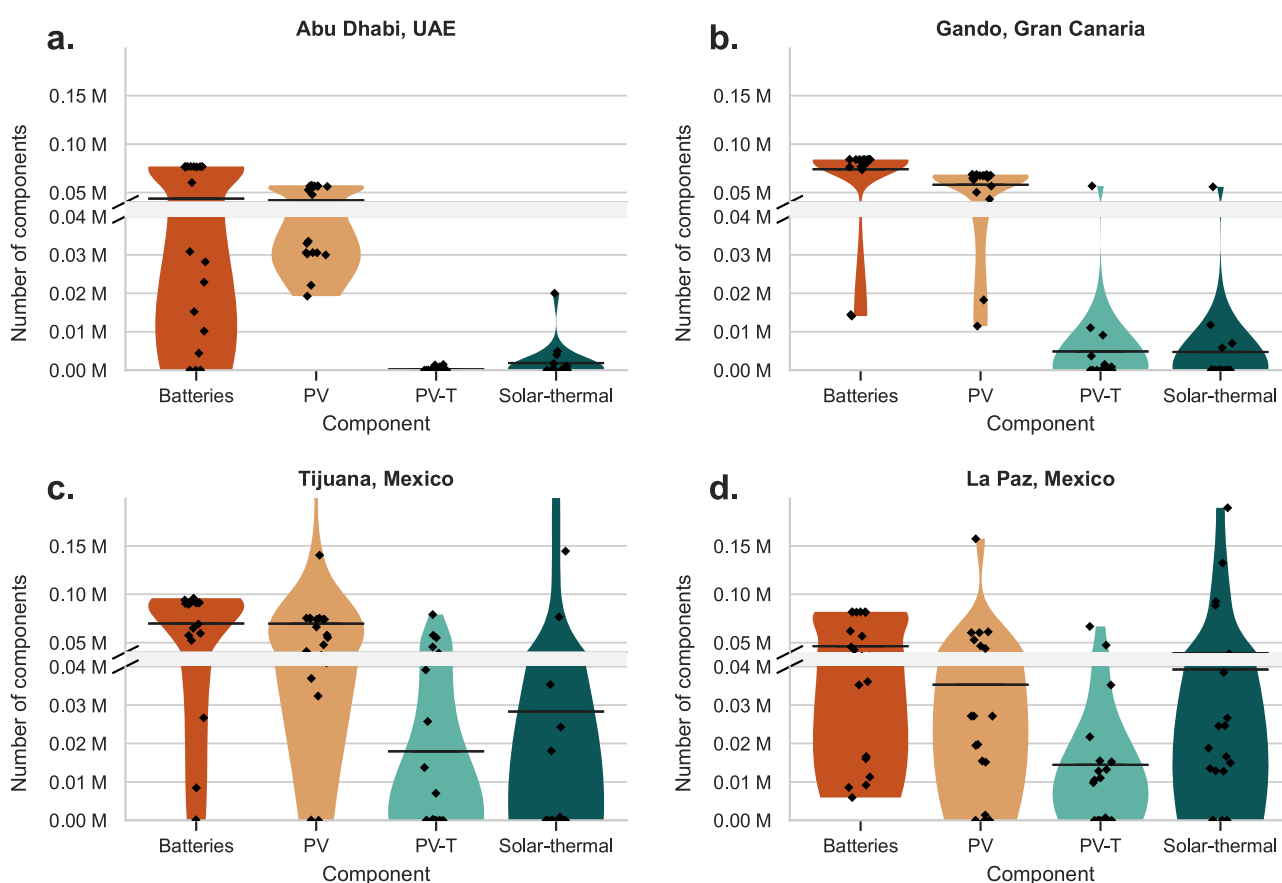


Fig. 2 | Installed components for the largest-scale MED plant. Scatter plot, along with an overlaid KDE in the form of a violin plot, of the number of batteries and PV, PV-T and ST collectors installed for 71 results (resulting from different component types and plant sizes) for the lowest total lifetime cost system for the largest-scale MED desalination plant considered. The mean value is marked by a black line. The plant considered is capable of outputting up to 1690 m³day⁻¹ of fresh water, the

specifics of which are detailed in Table 3. Results are shown for the four case-study locations considered: (a) Abu Dhabi, UAE, (b) Gando, Gran Canaria, (c) Tijuana, Mexico and (d) La Paz, Mexico. The results show an increase in system size across the four case-study locations considered correlated with an increase in the cost of grid-sourced electricity.

given in the Supplementary Tables. Results are disaggregated by plant size due to the three plants considered having specific costs which differed in magnitude and which could not easily be represented on a single figure.

Across all case-study locations, except Abu Dhabi, systems which utilised the p-Si panel modelled were associated with lower costs compared with those utilising m-Si collectors. Recent reductions in the

cost of m-Si PV modules, however, may lead to the lower costs than we found⁶⁵. By making our modelling open-source, we enable these analyses to be re-calculated as necessary as markets shift (<https://github.com/BenWinchester/HEATDesalination/>). More discussion on the implications of technology choice are given in the Supplementary Tables and Discussion.

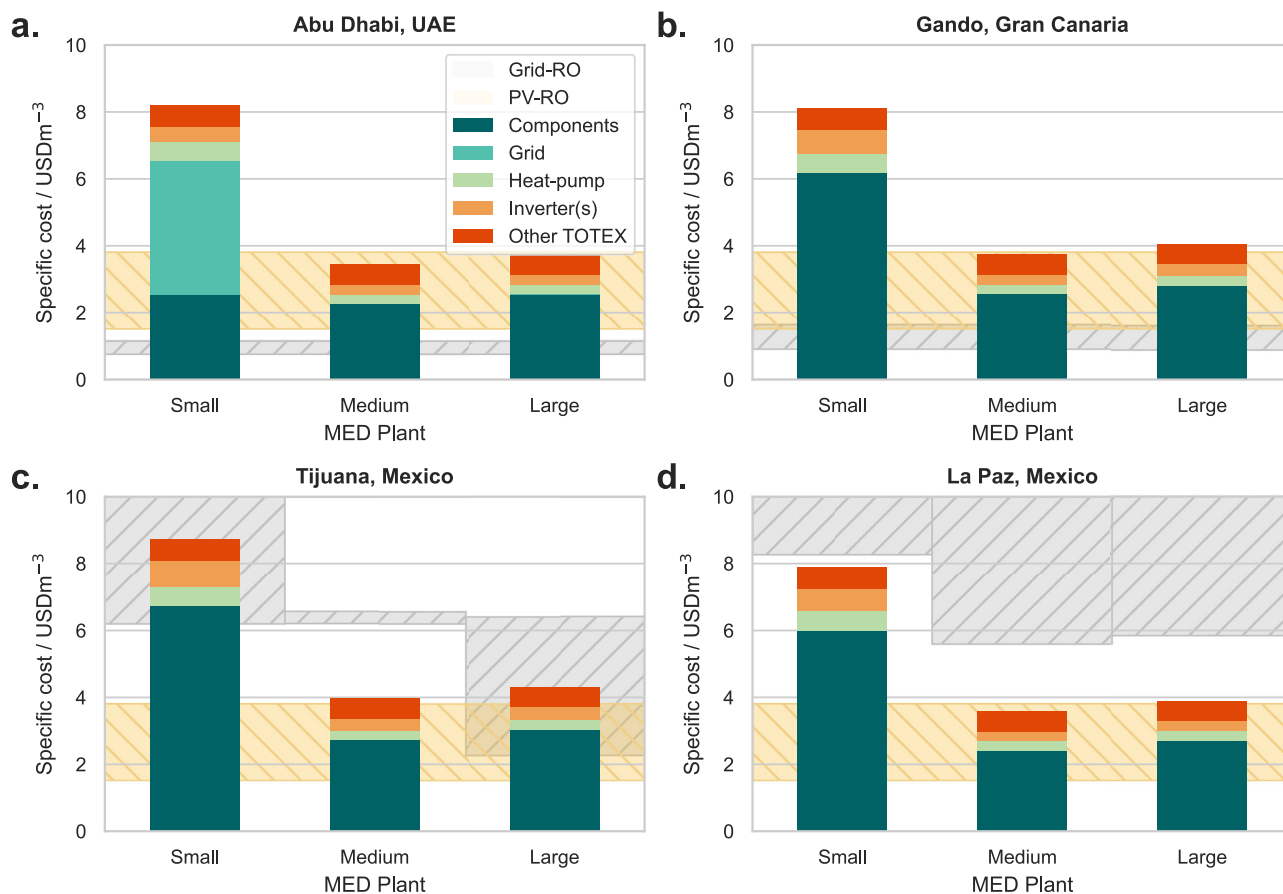


Fig. 3 | Specific cost of MED-desalinated water. Stacked-bar plot showing the specific costs of desalinated water for the lowest-cost configuration of components for the three MED plants considered. The bars are broken down vertically into component costs, the costs of grid-sourced energy, costs associated with the auxiliary heat pump and with the solar inverters, for each of the four case-study locations considered: (a) Abu Dhabi, UAE, (b) Gando, Gran Canaria, (c) Tijuana, Mexico and

(d) La Paz, Mexico. The specific costs associated with grid-driven and standalone PV- and battery-driven RO desalination are shown with grey- and yellow-hatched areas respectively. The embedded costs in the construction of the MED plant, as well as non-energy-related outgoings—such as staffing, repair and chemical pre-treatment of feedwater—are shown by the dark-orange section at the top of each bar.

Overall, we find that the technical specifications associated with the lowest-cost system depend on the reliance of the system on PV-T- and solar-thermal-driven heating as opposed to electricity-driven heat-pump heating with these trends being most pronounced for the smallest-capacity plant considered. The more expensive and higher-efficiency evacuated-tube collectors generally resulted in lower specific costs than the lower-cost and lower-efficiency flat-plate collectors considered. Poly-crystalline silicon PV modules were associated with systems with lower costs compared with mono-crystalline silicon (m-Si) collectors, though this may change as a result of recent reductions in the cost of m-Si panels which are not captured in the case-study panels considered here⁶⁵.

Sensitivity analysis

Due to the uncertainties in the lifetime of Li-ion batteries^{66–69} and solar inverters⁷⁰, we carried out sensitivity analyses where the inverter lifetime was varied between 1 and 29 years at 2 year intervals and the battery cycle lifetime was varied between 100 and 3000 cycles at 100-cycle intervals. Results of these analyses are presented in the Supplementary Figures.

Specific greenhouse gas emissions of desalination

The specific emissions for all three case-study plants across all four case-study locations, when optimised for the lowest lifetime cost, are shown in Fig. 5. The data show that, similar to the specific-cost data in Fig. 3, the specific emissions scale with the specific heat consumption of the plants. This is due to plants which require a greater amount energy per unit of

desalinated water needing a greater number of components and a larger amount of grid-sourced electricity, leading to higher specific emissions.

The data in Fig. 5 show that only the medium-scale MED plant in Abu Dhabi and Gando, and the medium- and largest-scale plants in La Paz, had specific emissions lower than, or comparable within error to, grid-powered RO. For Tijuana, the relatively low carbon intensity of electricity sourced from the grid ($310 \text{ gCO}_2\text{eqkWh}_{\text{el}}^{-1}$) results in MED plants having a higher specific carbon intensity than grid-powered RO. However, Fig. 3 shows that grid-powered RO in Tijuana is more expensive than either PV-RO or MED desalination, suggesting that grid-driven in RO in Tijuana, whilst less carbon intensive, may not be the most suitable choice.

Across all four case-study locations, Fig. 3 shows that solar-driven MED desalination is comparable within error to the emissions of PV-RO desalination for the medium- and largest-scale plants. This suggests that solar MED desalination can produce desalinated water comparable in both costs and emissions to PV-RO when optimised for the lowest lifetime cost. We attribute the relatively high emissions intensity associated with the smallest-scale system as being due to a combination of the higher specific energy consumption of the smaller-scale MED plant as well as the embedded emissions in the non-scalable system components. Additional analysis of Fig. 5 is given in the Supplementary Discussion.

Overall, when compared with grid-powered RO, a high grid emissions intensity of grid-sourced electricity or a low specific energy consumption of the plant can make MED desalination lower in both specific costs and emissions. This suggests that PV-, PV-T- and ST-driven MED desalination can produce clean water with both lower costs and emissions than grid-

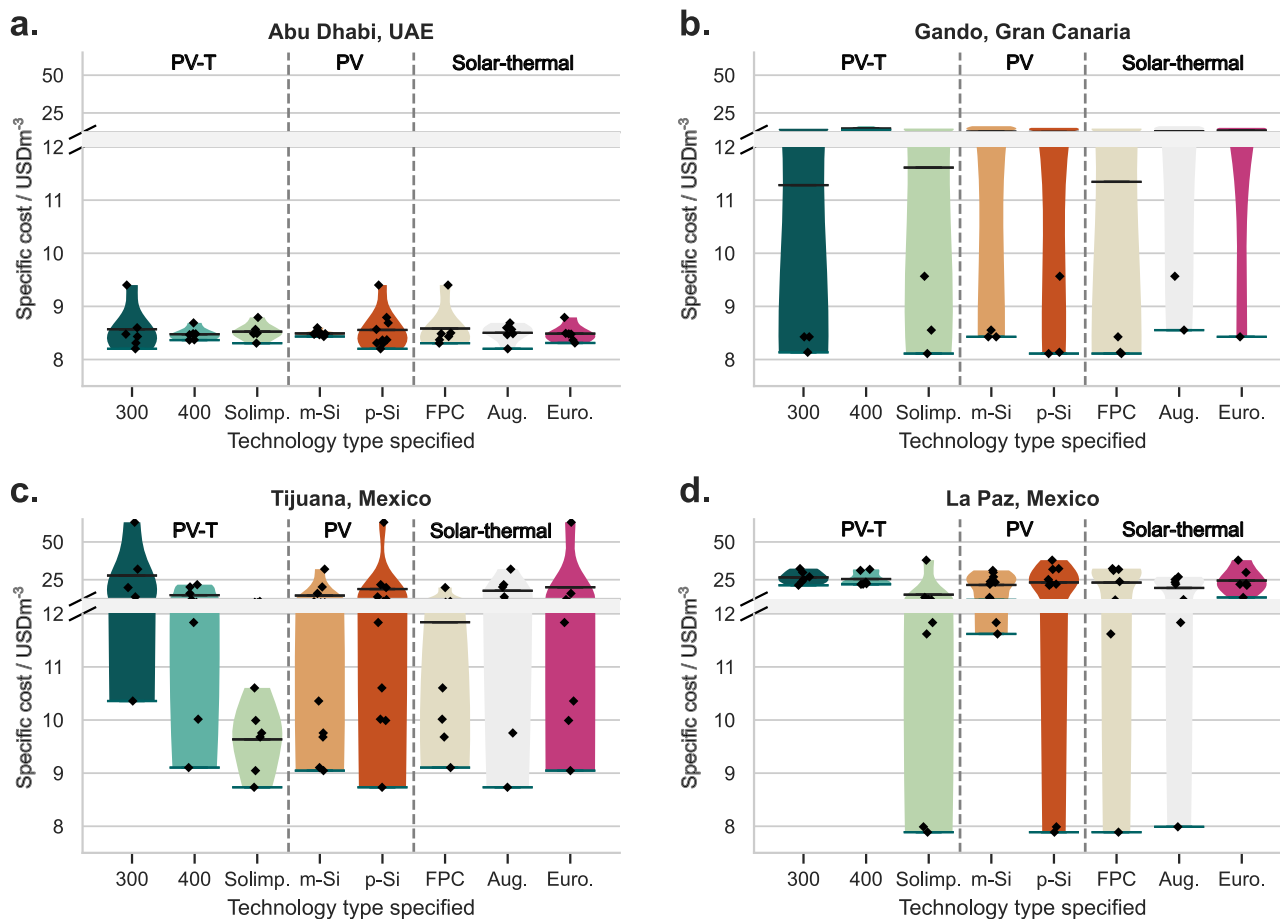


Fig. 4 | Effect of component choice. Scatter plot, along with an overlaid KDE in the form of a violin plot, of the total cost of the installed system over the lifetime of the smallest MED plant simulated⁴⁵. The mean and minimum values for each technology type are marked by horizontal black and red lines respectively. Vertical dashed grey lines demarcate the technologies into three groups: PV-T, PV and ST

collectors. For each result, a particular solar-collector technology was specified and results for the lowest lifetime cost aggregated over all other possible combinations. Results for all four case-study locations are shown: (a) Abu Dhabi, UAE, (b) Gando, Gran Canaria, (c) Tijuana, Mexico, and (d) La Paz, Mexico.

driven RO. Had we optimised for the lowest lifetime carbon emissions, the results would have produced systems of comparable or greater specific costs of clean water. Optimising for the lowest total lifetime carbon emissions of the plants, rather than the total lifetime cost as has been done here, may result in a greater number of systems that have a lower specific emissions associated than grid-powered RO though the associated costs will likely increase.

Comparison of specific cost results to the literature

Comparing with similar studies, the costs for the medium- (3.2–3.5 USDm⁻³) and large-scale plants (3.3–3.8 USDm⁻³) fall in the range of costs expected for solar-driven MED desalination utilising lower-temperature solar collectors (those which are non-concentrating in design): 4.1–14 USDm⁻³ found in a review by Zhang et al.⁵⁹, and 3.6–6.0 USDm⁻³ for an MED plant driven by ETC collectors in a review by Askari and Ameri⁶¹. Askari and Ameri found lower specific costs of clean water for a system driven by a combination of hybrid concentrated PV-T and ST collectors (2.9 USDm⁻³)⁶¹, though the lower costs found are likely due to their use of concentrating collectors. A recent study also found lower costs of solar-driven MED desalination of 0.45–3.1 USDm⁻³, but this was achieved through the use of hybridised MED plants⁶⁰, and so is not inconsistent with our results.

Whilst the costs found for the smallest-scale plant considered (7.0–7.6 USDm⁻³) are higher than those reported in some reviews, the output capacity of 3 m³day⁻¹ is smaller than many of the plant capacities produced and studied in the literature^{59,61}, so this would be expected due to

the economies of scale of such plants. In this context, the results found are consistent with those published in the literature.

Implications of national grid costs and component types for considering cost-competitiveness of MED

The cost of grid-sourced electricity greatly affects the specific cost and emissions of the clean water generated, the capacity of the optimum system installed, and the optimum balance between thermal and electrical heating. In Abu Dhabi and Gando, grid-powered RO is a more cost-effective means of supplying clean water than solar-driven MED desalination. In Tijuana and La Paz, this is reversed. These results are reflected in Fig. 3, where the MED plants are only lower in cost or cost-competitive within error in Tijuana and La Paz. PV-RO is cost-competitive within error for the medium- and largest-scale MED plants and produces water with a lower specific cost than the smallest-scale plant across all four case-study locations.

The price of grid-sourced electricity hence has the greatest impact on which desalination technology, whether electrically-driven RO or thermally driven MED, can produce clean drinking water at the lowest specific cost. Given grid prices vary, both geographically and over time, it is necessary for manufacturers and stakeholders to carefully model their system to determine the most cost-effective system for their specific case.

The specific cost of desalinated water produced is a key factor for decision makers. However, the required performance of any desalination system also needs to be taken into consideration. Whilst RO may be able to produce desalinated water at a lower cost than thermally driven technologies, the nature of the process results in lower-quality product water than

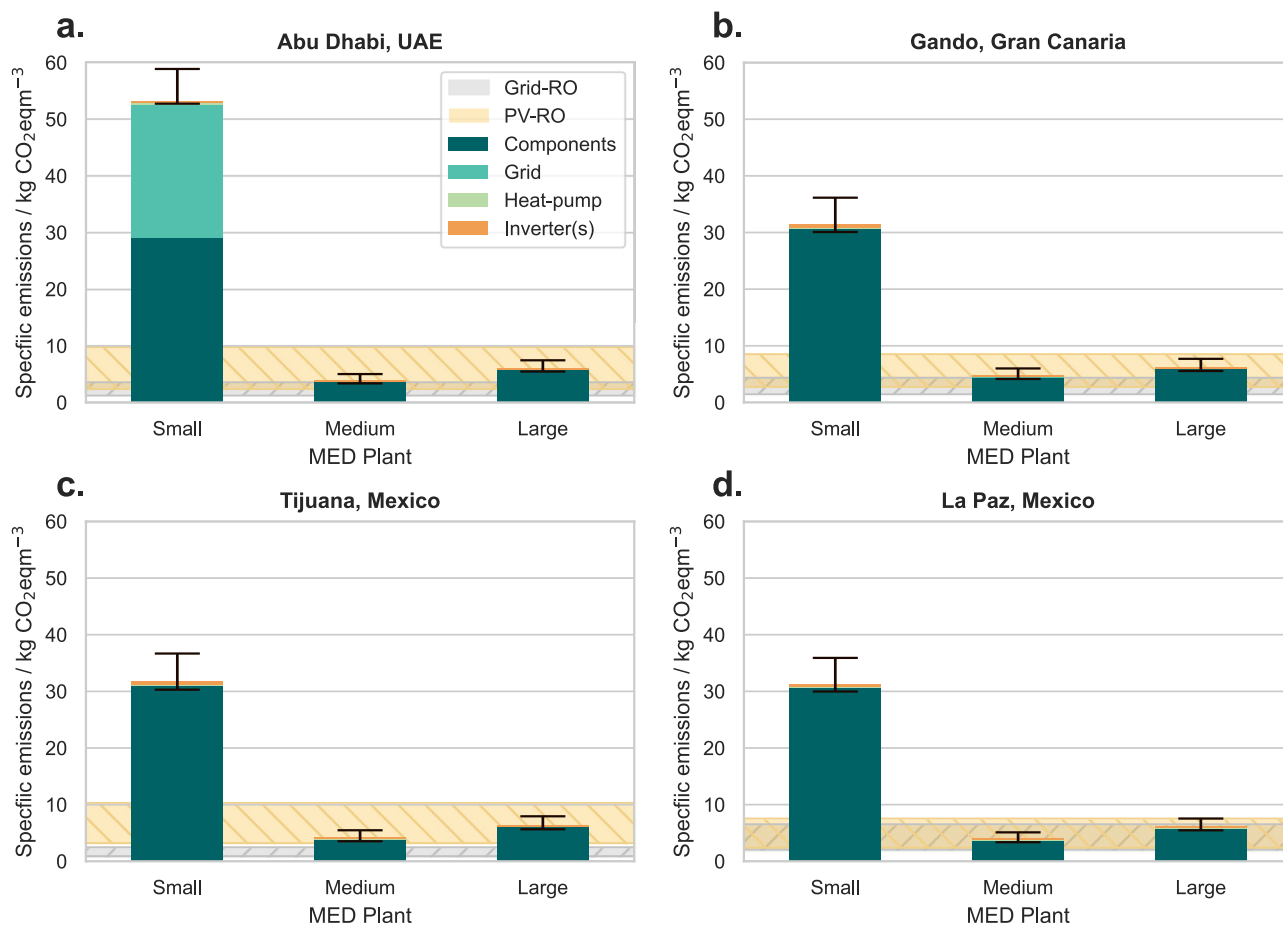


Fig. 5 | Specific emissions of MED-desalinated water. Stacked-bar plot of the specific emissions resulting from energy generation for each of the three plant capacities when optimised for the lowest lifetime cost in each of the four case-study locations: (a) Abu Dhabi, UAE (b) Gando, Gran Canaria, (c) Tijuana, Mexico and (d) La Paz, Mexico. The specific emissions resulting from grid-driven and PV-and-battery-driven RO desalination are shown with grey- and yellow-hatched areas respectively. The black error bar contains uncertainty in the emissions estimates as

well as embedded emissions. Uncertainty in the emissions resulting from grid-powered RO arises from the range of specific energy-consumption values for RO used: 2–7 kWh_{el}⁵⁶. Uncertainty in the emissions associated with the batteries and inverters, detailed in the Methods, along with a 10% margin for emissions resulting from the MED plant infrastructure²⁰, result in the error bars visible. An estimate for the embedded emissions in the construction of the MED plant are accounted for in the black error bar also.

thermally driven processes^{29,41}—up to 500 ppm salt content as opposed to less than 10 ppm for MED. Although MED is feedwater agnostic, RO requires more complex pretreatment systems to avoid issues such as membrane fouling^{71,72}. Further, the salinity of the product water increases with the salinity of the input water used⁷³. Taken together, despite the lower specific cost of electrically-driven RO, including in Abu Dhabi and Gando where our study is focused, it may not always be the best technology choice for desalinating high-salinity salt water due to implications on the quality of product water and the risks associated with membrane fouling.

The choice of collectors used had a specific impact on the cost of clean water produced. This is most pronounced in La Paz, where the cost of grid-sourced electricity was the highest and where systems were primarily self-reliant (see Fig. 1). The lifetimes of the components (batteries and solar-charge inverters) also affected the balance between self-generated and grid-sourced electricity. It is hence necessary to consider the available collectors, not on the most efficient designs, as well as the various batteries and inverters available when commissioning a plant.

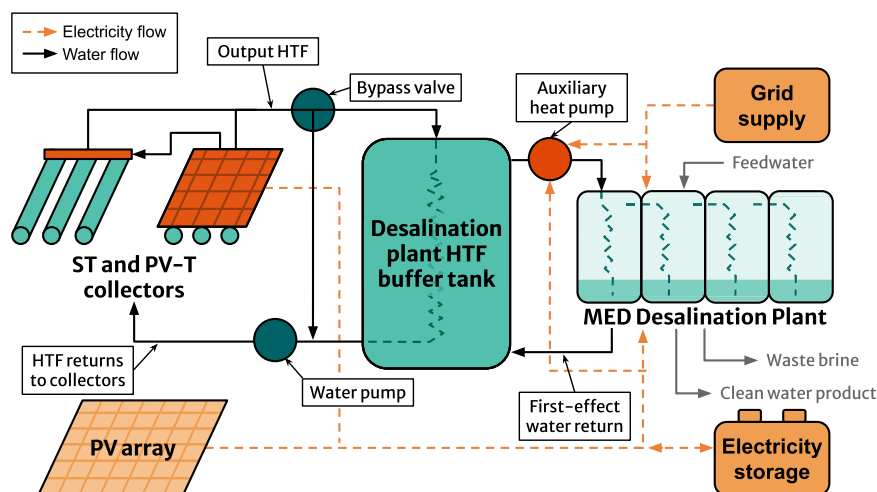
The results in Fig. 5 show that optimising for the lowest lifetime cost results in systems that are higher in emissions than grid-powered and PV-driven RO in all case-study locations bar La Paz, where the emissions intensity of grid electricity is the highest of the case-study locations considered. Solar-powered MED desalination does not therefore necessarily produce lower emissions than grid-driven RO

despite using renewable solar collectors and producing lower-cost desalinated water. The emissions are generally lower than, or within error of, those arising from PV-RO systems for the medium- and largest-scale desalination plants. Optimising for the GHG emissions produced may result in MED systems that have lower emissions than both grid-powered and PV-driven RO whilst not sacrificing considerably on cost.

Overall, we present an open-source integrated model for the lifetime optimisation of the configuration of photovoltaic (PV), hybrid photovoltaic-thermal (PV-T) and solar-thermal (ST) systems, as well as battery storage, the mass flow rate of heat-transfer fluid, and the capacity of thermal storage installed, for a multi-effect distillation (MED) plant. of the space of commercially-available technologies⁷⁴, as well as three MED plant capacities ranging from community-scale (3 m³day⁻¹⁵⁵ and 30–60 people per day³⁷) to municipal-scale (1964 m³day⁻¹⁵⁸, up to 33000 people per day³⁷). We make our model open-source so that other stakeholders, manufacturers, and industry experts can utilise our methodology to consider components particular to their needs for optimising and simulating the performance of such systems over the lifetime of plants of various capacities (<https://github.com/BenWinchester/HEATDesalination/>). Further, by doing so, we provide scope for investigating nascent technologies such as smaller-scale membrane distillation³³ within the framework developed. We optimised the configuration of the systems based on the lowest total lifetime cost incurred.

Fig. 6 | MED plant considered in the study.

Schematic showing the system configuration for the MED plant modelled. A series of PV-T and ST collectors are connected in series such that a HTF, taken in this case to be water, first passes through the PV-T and then the ST collectors. The HTF passes through a buffer tank containing water which is then used to supply heat to the MED desalination plant. A PV array, if present, in conjunction with the electrical output from the PV-T collectors, supplies the electrical needs of the plant, with electrical storage in the form of batteries stores excess power generated. A grid supply meets any shortfall in the electrical power supplied by the renewable PV and PV-T collectors.



Methods

We consider a combination of PV-T, PV and ST collectors, in conjunction with electrical and hot-water storage, and a grid connection, for the provision of electricity and heat for an MED desalination plant. An air-water heat pump is used to meet auxiliary heating demands.

We developed an integrated model of the solar collectors with hot-water storage tanks to determine their electrical and thermal outputs. We consider here only ST flat-plate collectors (FPCs) and evacuated-tube collectors (ETCs). We make our software open-source and available online so other designs can be explored (<https://github.com/BenWinchester/HEATDesalination/>).

We implemented an optimisation algorithm, making multiple target variables, including the lowest lifetime cost and emissions, available (<https://github.com/BenWinchester/HEATDesalination/>). We utilised this to determine system configurations and technologies that resulted in the lowest total cost over the lifetime of selected MED plants. For the total cost, we included the costs of the initial energy-generation equipment and any replacements necessary, as well as the costs of grid electricity. Additional costs associated with the plants were not included as they are plant-dependent and are not affected by the size of the energy-generation system installed. We include these under the label “other TOTEX.”

For the carbon dioxide equivalent (CO_2eq) emissions associated with the MED plants, we consider both the embedded emissions in the technologies installed, as well as the ongoing emissions arising from electricity sourced from the grid. Where uncertainty exists in the literature, we have considered upper- and lower-bound estimates on these values. The embedded emissions in the plants have also been considered, though these are not calculated as part of the optimisation tool as they are independent of the energy-generation system and are, instead, added afterwards.

In the next sections, we present the details of the modelling and input parameters used to assess the performance of the PV, PV-T and ST collectors as well as the electrical battery storage considered.

Modelling solar technology performance

We here model ST, PV-T and PV collectors. For hot-water generation, we consider PV-T and ST collectors, either connected in series (PV-T followed by ST collectors) or as independent technologies. Thermally-coupled PV-T collectors are limited in their fluid temperatures compared with thermally-decoupled designs. For thermally-coupled collectors, higher fluid temperatures result in both a lower electrical efficiency as well as a greater risk of damage to the PV cells^{75,76}. Thermally-decoupled spectral-splitting collectors⁷⁷, or partially-laminated collectors⁷⁸, are two approaches to mitigate these issues. One recent solution that utilises readily available collectors employs PV-T and ST collectors connected in series such that high output temperatures from the collector system can be achieved whilst

reducing the output temperature of the PV-T collectors and hence the temperature of the PV cells⁷⁹.

The same approach is used to model the thermal performance of the PV-T and ST collectors. This is outlined in the Supplementary Methods. The electrical performance of the PV-T and PV panels is modelled differently. These approaches are outlined in the Supplementary Methods also.

MED desalination plant model

A schematic of the desalination plant and solar generation system is shown in Fig. 6. We consider an MED desalination plant such that hot water from a buffer tank is drawn through a pipe within the first effect. We assume continuous operation of the plant. Hence, a steady amount of water is drawn from the buffer tank and passed through the first effect of the MED system before returning to the buffer tank at a cooler temperature. If the temperature of the water leaving the buffer tank is less than the desired hot-water temperature of the plant, it is heated using an electrically-driven heat pump.

PV-T and ST collectors, if present, are used to heat the water within the buffer tank. An HTF passes through the PV-T (if present) and ST (if present) collectors in turn. If the HTF leaving the collector system is higher in temperature than the fluid within the buffer tank, it flows through a heat exchanger and transfers heat to the tank. Otherwise, a bypass valve redirects the fluid back through the collector system.

We here consider lithium-ion (Li-ion) batteries, the characteristics for which are given in Table 2. An efficiency of 95% was used for both charging and discharging, resulting in a roundtrip efficiency of 90%. This is higher than values obtained by Bobanac et al.⁸⁰, who accounted for columbic efficiency, for a *c*-rate of 0.6, but will vary greatly between manufacturers and due to cycling conditions⁸¹, so is taken here as a reflective estimate. The costs for the batteries given in Table 2 were accurate at the time of writing and are reported at the level of precision included within the modelling. The lifetime capacity loss of the batteries was based on 24% degradation for 500-cycle batteries reported by Spotnitz et al.⁶⁶ and < 20% for 4500-cycle batteries reported by Yang et al.⁶⁷

Any shortfall in electrical demand, which cannot be met directly with PV- or PV-T-generated electricity or from battery storage, is made up by supply from the grid, the costs of which vary between locations and which are given in Table 8. Grid-infrastructure costs are neglected due to these varying significantly from country to country and between locations, though, should these be needed by stakeholders, scope is provided to include these in the open-source model (<https://github.com/BenWinchester/HEATDesalination/>). We assume a 30 year plant lifetime, common across the type of plants considered. The optimum tilt angles for the collectors, given in Table 8, were obtained from Huld et al.⁸². The cost of grid-sourced electricity on Gran Canaria ($0.146 \text{ USD kWh}^{-1}$) was taken from Qiblawey et al.⁵⁴.

We considered three different capacities of desalination plants, capable of producing 3, 120, and 1700 m³ of freshwater per day respectively. The properties of these plants are given in Table 3. The electrical power consumption of the plants is calculated based on their daily freshwater-output capacities and the average specific MED power consumption^{40,41}.

To assess the electrical load placed on the system by heat-pump-driven auxiliary heating, we convert the thermal load placed on the heat pump into an electrical load that it places on the system. Details on the modelling used are given in the Supplementary Methods. The heat pump will operate with a condensation temperature slightly higher than the hot-water temperature required by the MED plants, and with an evaporation temperature slightly lower than the ambient temperature. More detail on the temperature difference utilised is given in the Supplementary Methods.

Table 2 | Technical parameters of the Lithium-Ion battery used in the modelling

Manufacturer Model	Renogy ^a 12V 100Ah
Capacity (Q_{max}) / kWh	1.28
Charging efficiency	0.95
C-rate, charging (cr_{chg})	0.58
C-rate, discharging ($cr_d - chg$)	1.0
Cost / USD/component	495 ^a
Cycle lifetime (N_L) / cycles	2000
Depth of discharge (DoD) / %	80
Discharging efficiency	0.95
Leakage / %/hour	0.00417
Lifetime capacity loss d_L / %	0.241

^ahttps://uk.renogy.com/12v-100ah-lithium-iron-phosphate-battery-w-bluetooth/?gclid=CjwKCAIA85efBhBbEiwAD7oLQOyzKacstrf6R5tHfi5zGtBWxOKTydER-UDARqykjAsu6LakT1LExoCxtQQAwd_BwE

Table 3 | Specifications of the case-study multi-effect distillation (MED) desalination plants used

Name	$\dot{m}_{prod} / m^3 day^{-1}$	P / kW_{el}	\dot{m}_{hw} / kgs^{-1}	$T_{hw} / ^\circ C$	$T_{hw,r} / ^\circ C$
Small	3	0.288	0.919	75	65
Medium	120	11.5	3.75	77	31
Large	1700	107	100	80	54

Table 4 | Costs of the solar collectors used in the study

Collector type	Manufacturer	Model	Cost / USD-per-collector
Solar thermal	Solar Technologie International GmbH	FKF 240 V CuCu	494
	soldirekt24 GmbH	Eurotherm Solar Pro 20	631
	Augusta Solar	AS 100 DF	925
Photovoltaic-thermal	Dualsun	(insulated) Spring 300M	566 ^a
	Dualsun	(insulated) Spring 400M	1020 ^b
	Solimpeks	Powervolt	545
Photovoltaic	REC	325 N-Peak Mono	155
	Sharp	ND-AF 330 C	112

Cost information was sourced either directly from the manufacturers or from Olympios et al⁷⁴, and was correct at the time of writing.

^aCost value taken at the time of modelling from ClimaVerd (<https://www.climaverd.com/productos/termo-fotovoltaica/tproduct/250779776-344696527841-dualsun-spring-300m-aislado-pvt>).

^bValue taken from the Dualsun 2023 catalogue (<https://my.dualsun.com/wp-content/uploads/sites/2/dualsun-en-product-system-catalogue.pdf>).

Component costs

Component costs for the various collectors used are given in Table 4. The costs of the hot-water tanks installed, electrical storage, and solar-power inverters used are given in Table 5. The hot-water tank was taken from Olympios et al.⁷⁴ whilst the inverter was taken from Sangwongwanich et al.⁷⁰. We selected the battery based on typical costs and capacities for Li-ion based batteries, and costed the inverter based on typical inverter costs (<https://www.zerohomebills.com/product/solis-6kw-solar-inverter-w-dc-isolator/>) and selected a lifetime of 13 years based on that for a dry-and-hot climate⁷⁰. We selected the hot-water tank used based on the lowest standard deviation from the mean cost per unit energy stored, as found by Olympios et al.⁷⁴, and among the lowest values for the seasonal daily heat loss. The model is able to size the hot-water storage system by altering the number of these tanks installed.

For the costs of the desalination plant which do not arise directly from the energy-generation system—including the capital costs in construction of the plant along with operation costs such as repairs, staffing and chemicals used in the pre-treatment of the feedwater—we take values from Rahimi et al.⁵⁸. We include the values given in the study and adjust for inflation to calculate specific costs of 0.65, 0.61 and 0.57 USDm⁻³ for the smallest-, medium- and largest-scale plants modelled respectively. These are shown by the solid orange bars in Fig. 3.

Model of component degradation

We degrade the electrical performance of the PV and PV-T collectors and the installed batteries over their lifetime using an average degradation rate of 1.1% year⁻¹ in efficiency for PV modules⁸³ and manufacturer-specific

Table 5 | Capacities and costs of the batteries, hot-water tank(s) and inverter(s) installed

Component	Heat-transfer fluid pump	Hot-water tank	Inverter
Manufacturer	Grundfos	Grant	Solis
Model	CRNF 15-1 A-CA-A-E-HQQE	HPMONO/IND150	S5-GR1P6K 5G
Capacity	20.5 m ³ h ⁻¹	150 l	6 kW
Cost / USD/component	4170	1250	890 ^a
Reference	Grundfos website ^b	^c	^c

^aThe inverter was costed based on typical solar-PV inverter costs (<https://www.zerohomebills.com/product/solis-6kw-solar-inverter-w-dc-isolator/>).

^bThe heat-transfer fluid pump data was based on data obtained from the Grundfos website (<https://product-selection.grundfos.com/uk/products/crnfex/crnf-15-1-98415336?tab=variant-specifications&pumpsystemid=2024447336>).

^cReferences provided within the main text.

Table 6 | Summary of weather environmental conditions for the four case-study locations

Location	Mean temp. / °C	Daily temp. standard deviation / °C	Seasonal temp. standard deviation / °C	Max. irradiance ^a / Wm ⁻²	Input water type ^b
Abu Dhabi	28.1	2.92	6.19	945	SW
Gando	20.3	0.25	2.18	856	SW
Tijuana	16.2	2.08	3.27	844	BW/SW
La Paz	23.9	4.13	4.42	932	SW

^aThe average daily irradiance is utilised in the modelling. The maximum hourly irradiance achieved is given as an indicator of the peak summer-time solar resource available.

^bThe sources of water for desalination, whether brackish water (BW) or saltwater/seawater (SW).

Table 7 | Currency exchange rates used to adjust financial inputs

Exchange rate	Value
British-pound-to-dollar / USD-per-GBP (British Pound)	1.38 ^{a,b}
Euro-to-dollar / USD-per-EUR (Euro)	1.05 ^c
UAE-Dirham-to-dollar / USD-per-AED (Arab Emirates Dirham)	0.27 ^d

^aThe rate of inflation was taken from the Bank of England's inflation calculator (<https://www.bankofengland.co.uk/monetary-policy/inflation/inflation-calculator>).

^bThe exchange rate between British Pounds and United States Dollars was obtained from the UK Office for National Statistics (<https://www.ons.gov.uk/economy/nationalaccounts/balanceofpayments/timeseries/auss/mret>).

^cThe exchange rate between Euros and United States Dollars was obtained from the website of the European Central Bank (https://www.ecb.europa.eu/stats/policy_and_exchange_rates/euro_reference_exchange_rates/html/eurofxref-graph-usd.en.html).

^dThe exchange rate between Arab Emirates Dirhams and United States Dollars has been fixed since 2014 when the UAE Dirhama was pegged to the dollar.

degradation values for the batteries considered. Details on the methods employed are given in the Supplementary Methods.

In the next sections, we outline the case-study locations considered, including the costs associated with grid-sourced electricity in each location, as well as the nature of the optimisation process employed. Details on the benchmarks used for assessing the performance of the MED systems against the more-commonly-employed RO desalination follow.

Case-study locations and environmental conditions

We took four case-study locations which rely on desalination to meet a portion of their clean-water demands and which varying proportions of fossil fuels within their energy mixes: Tijuana and La Paz in Mexico, Abu Dhabi in the United Arab Emirates (UAE), and Gando on Gran Canaria, Spain. We selected this range of locations to study the effect of grid and component costs, as well as the ambient temperature and solar irradiance, details of which are given in Table 6, on the optimum system.

Due to the high variability in the price of grid electricity throughout Mexico⁸⁴, we selected two locations within the states of Baja California and Baja California Sur which represented the extreme grid-electricity costs—with up-to-date values taken from the website of the Comisión Federal de Electricidad (<https://app.cfe.mx/Aplicaciones/CCFE/Tarifas/TarifasCRENegocio/Negocio.aspx>)—across the country⁸⁴, Tijuana and La Paz, both of which have a high risk of suffering from droughts⁸⁵ and have high and medium water-scarcity indices respectively^{86,87}. Further, Tijuana remains the site of an un-built government-priority desalination plant⁸⁸.

We use the site of an existing solar-thermal-powered desalination plant near Abu Dhabi, capable of producing 120 m³ day⁻¹ of fresh water, as the source of our UAE-based environmental data⁵⁷, the specifics of which are given in Table 3. With the sixth-highest per-capita carbon emissions as of 2021⁸⁹, and the fourth-lowest per-capita renewable-water resource as of 2018 (<https://ourworldindata.org/water-use-stress>), the UAE relies on seawater desalination to satisfy over 50% of its freshwater demand³².

There is variability in the primary source of drinking water across the Canary Islands, with the easternmost islands, including Gran Canaria, reliant on desalination as their primary source of drinking water⁹⁰. Despite a shift towards renewable energy-generation technologies, only 16% of the electricity demand of Gran Canaria was generated renewably in 2019⁹¹. The remaining share was met through carbon-intensive fuel- and gas-oil plants. Fewer than 1% of desalination plants across the archipelago were powered by at-site renewable technologies as of 2019⁹².

We obtained weather data, along with optimum panel tilt angles, for the various locations chosen using the publicly-available PVGIS database⁸². This, along with the latitude and longitude of sites used and the cost of grid electricity, is given in Table 8. Exchange rates to the USD have been applied for British Pounds, Euros and Abu Dhabi Dhirsams. These are given in Table 7. We obtained the latest grid-cost information for Tijuana and La Paz from the Comisión Federal de Electricidad (<https://app.cfe.mx/Aplicaciones/CCFE/Tarifas/TarifasCRENegocio/Negocio.aspx>). The tiered pricing structure used is given in Table 9 for Tijuana and La Paz.

The price of grid-sourced electricity changes over time, both as markets fluctuate⁹³, and as the renewable-electricity mix changes⁹⁴. Due to uncertainties in predicting future electricity prices, we took the costs of grid-sourced electricity to be constant throughout the lifetime of the plant. Similarly, we chose not to apply discount rates to the batteries and solar inverters modelled to be in-keeping with our approach to grid costs.

Optimisation approach

We aim to optimise the energy-generation system, consisting of PV, PV-T and ST collectors with electrical and hot-water storage, for the lowest lifetime cost. We do so by varying the capacities of components installed, and hence the reliance on grid-sourced electricity and auxiliary heating, whilst fixing component costs and environmental conditions. We allow for a variable and optimisable global mass flow rate through the thermal-collector system as well as a varying buffer-tank capacity.

We undertook an analysis of optimisation algorithms and selected two based on their ability to successfully determine the optimum component sizes for the system when compared with the results of a global optimisation: the Nelder-Mead (N-M)⁹⁵ and Limited-memory Broyden-Fletcher-Goldfarb-Shanno (L-BFGS-B)⁹⁶ algorithms.

We minimise the system based on the lowest total lifetime cost, where both the initial equipment investment costs and the ongoing cost of grid electricity are considered. We provide other target variable for optimisation, such as the LCOE, grid-electricity fraction and auxiliary- and renewable-heating fractions, in our open-source code depending on the needs of various stakeholders (<https://github.com/BenWinchester/HEATDesalination/>).

Sensitivity analysis

Despite the potential for Li-ion batteries in renewable-energy contexts⁹⁷ and recent attempts to improve degradation modelling⁹⁸, there remain uncertainties around the impact of environmental conditions, deep discharging and overcharging on both their cycle lifetime and lifetime capacity loss⁶⁶⁻⁶⁹. Uncertainties also exist around the lifetime of solar inverters, where climatic conditions can result in a five-fold variation in lifetime⁷⁰.

To account for this uncertainty, we carried out a sensitivity analysis in which we varied the cycle lifetime of the Li-ion batteries and solar inverters

Table 8 | Position, grid-cost and solar-collector tilt values for locations studied

Location	Latitude / °N	Longitude / °E	Grid cost / USDkWh _{el} ⁻¹	Tilt / °
Abu Dhabi, UAE	24.44	54.49	0.078 ^a	24
Gando, Gran Canaria	27.94	-15.37	0.146	25
Tijuana, Mexico	32.49	-117.11	See Table 9	32
La Paz, Mexico	24.17	-110.29	See Table 9	24

^aCost data for Abu Dhabi obtained from the Abu Dhabi Distribution Co. Rates and tariffs 2018 website (<https://www.addc.ae/en-US/business/Pages/RatesAndTariffs2018.aspx>).

Table 9 | Tiered grid-cost structure used for case-study locations, Tijuana and La Paz, in Mexico, obtained from the Comisión Federal de Electricidad

Location	Tariff	P_p / kW	C_f^a / USD-per-month	C_{cons}^b / USDkWh ⁻¹	C_{cap}^c / USDkW _p ⁻¹
Tijuana	PDBT	<25	59.90	2.47	0
Tijuana	GDBT	>25	599	0.826	499
La Paz	PDBT	<25	59.90	3.82	0
La Paz	GDBT	>25	599	2.91	454

The costs shown were accurate at the time of writing and are reported at the level of precision included within the modelling.

^a C_f is a fixed monthly cost for a commercial connection to the national grid network.

^b C_{cons} is a consumption-based cost per unit electricity consumed, charged monthly.

^c C_{cap} is a capacity-based cost, charged based on the peak power demand within a month.

modelled. Sensitivity to other parameters, such as the costs of various components and electricity sourced from the grid, is partially accounted for by the different case-study components and locations considered respectively. Results of the sensitivity analyses are given in the Supplementary Figures whilst results of the impact of technology choice amongst different commercially-available collectors are contained within the Supplementary Tables and Discussion.

Lifetime-emissions analysis

To determine the desalination system best able to provide clean water in line with the United Nations SDGs²¹, it is necessary to quantify, not only the costs, but also the environmental impact of these systems. For their climate-change impact, we quantify this in terms of their embedded carbon dioxide equivalent (CO₂eq) emissions. Detailed information on the methodologies and inputs used to determine the associated emissions of the systems are given in the Supplementary Methods.

Reverse-osmosis benchmark model and inputs

As RO is the most deployed desalination technology globally^{32,33}, we calculated the specific emissions and costs of using RO to meet an equivalent clean-water demand to the plants modelled, the specifics of which are given in Table 3. There is a range reported in the literature in terms of the energy consumption of RO⁵⁶. We reflect this range by estimating a range of values for the costs and emissions of these systems.

For the RO system, we include capital infrastructure costs, operation and maintenance costs (including membrane replacement, etc.) as well as the costs of the energy generation system in the estimates produced. For the CAPEX and non-energy OPEX costs associated with RO desalination, we use a fixed value of 0.60 USDm⁻³ based on 2022 data calculated by Ghaithan et al.⁹⁹.

For the grid-powered RO benchmark, we compute the associated lifetime electricity consumption for powering an RO unit through grid electricity. The embedded emissions associated with grid electricity, given in the Supplementary Methods, are used to calculate an upper-bound estimate for the lifetime emissions as the carbon intensity of grid-sourced electricity is likely to decrease over time as countries decarbonise.

As 43% of renewably-powered desalination was performed using PV-RO as of 2020²⁸, we used PV-RO as a further benchmark for the lifetime costs and emissions. To calculate the size of PV-and-battery system needed to carry out desalination independent of a grid connection, we used estimates for the energy consumption of RO units from Ghaithan et al.⁹⁹ of 2–7 kWh_{el}m⁻³. We used their specific energy costs and adjusted these for this range to produce estimates for the specific costs of PV-RO water of 1.5–3.8 USDm⁻³. These values fall within the range of values presented by Caldera et al. in their 2018 handbook of salt-water RO costs (1.0–4.2 USDm⁻³) and are hence consistent with the wider literature¹⁰⁰.

For the emissions arising from the CAPEX and non-energy RO components, such as membrane replacement and chemical pre-treatment, we take a range of values of 0.299–0.320 kgCO₂eq based on the breakdown produced by Shahabi et al.¹⁰¹. Taken together, these estimates provide a range of values for the specific costs and emissions associated with RO desalination, whether grid-powered or PV-driven. These estimates are used as a benchmark to compare the performance of our MED system against.

Limitations

There are a few limitations in the modelling approach used, primarily in terms of how discount rates and costs are treated, as well as the nature of the simulation and optimisation approaches undertaken. These limitations, and their impact on the study, are outlined here.

The price of the grid electricity used for the case-study locations considered, detailed in Tables 8 and 9, will change over time, both on a daily basis, as the hourly renewable energy resource available and real-time demand placed on the grid affect the cost of purchasing electricity from the grid, and on a longer-term scale as countries introduce legislation and aim to decarbonise their grids. In this work, we assumed that the cost of grid-sourced electricity was unchanging over the lifetime of our plant. Ignoring the longer-term effects may result in an outcome which favours self-reliant systems due to current high prices of grid electricity making these systems unattractive. On a shorter time scale, we selected case-study locations with a fixed tariff, i.e., one which does not vary depending on the environmental conditions. As such, the model developed is limited in its current scope to a static price of grid electricity but is not limited in this regard.

The costs of components will also change over time and, if historic trends continue, are likely to decrease for solar PV panels¹⁰² and Li-ion batteries¹⁰³. In-keeping with the approach taken for the cost of grid electricity, we considered only static costs for the various components installed. This is likely to result in battery storage being a less favourable means of providing night-time electricity than grid-sourced power as, when batteries are replaced, they will be replaced at the original price used at the start of the simulation period, rather than the discounted price. This effect will be in competition to the impact of considering a static non-decreasing grid-electricity price.

A further limitation exists in the choice of optimisation algorithm. The nature of the optimisation algorithms employed here means that local, rather than global, optima are found^{95,96}. These approaches thus reduce the computation time for generating results at the cost of determining the global lowest-cost system. Further, N-M and L-BFGS-B algorithms result in non-integer solutions due to the continuous nature of the optimisation variables. To mitigate this, after the optimisation process has been completed, we considered all permitted integer results surrounding the optimum point and

selected that with the most optimum value depending on the optimisation criterion being minimised or maximised.

Data availability

All relevant data used in this study are available from the authors. The datasets generated and analysed during the study are available on Zenodo, and can be accessed via this link: <https://doi.org/10.5281/zenodo.7801892>.

Code availability

The underlying code for this study is available on GitHub in BenWinchester/HEATDesalination and can be accessed via this link: <https://doi.org/10.5281/zenodo.7612965>.

Received: 24 November 2023; Accepted: 14 May 2024;

Published online: 16 July 2024

References

- United Nations Children's Fund (UNICEF). *1 In 3 People Globally Do Not Have Access To Safe Drinking Water*. <https://www.unicef.org.uk/press-releases/1-in-3-people-globally-do-not-have-access-to-safe-drinking-water-unicef-who/> (2019).
- Cozzi, L., Wetzel, D., Tonolo, G., Diarra, N. & Roge, A. *Access To Electricity Improves Slightly In 2023, But Still Far From The Pace Needed To Meet SDG7*. <https://www.iea.org/commentaries/access-to-electricity-improves-slightly-in-2023-but-still-far-from-the-pace-needed-to-meet-sdg7> (2023).
- Cozzi, L., Wetzel, D., Tonolo, G. & Hyppolite, J. II. *For The First Time In Decades, The Number Of People without access To Electricity Is Set To Increase in 2022*. <https://www.iea.org/commentaries/for-the-first-time-in-decades-the-number-of-people-without-access-to-electricity-is-set-to-increase-in-2022> (2022).
- International Energy Agency (IEA). *Electricity Market Report - July 2021*. <https://www.iea.org/reports/electricity-market-report-july-2021> (2021).
- IEA. *Global Energy Review 2021*. IEA, Paris <https://www.iea.org/reports/global-energy-review-2021> (2021).
- Hasanuzzaman, M., Zubir, U. S., Ilham, N. I. & Seng Che, H. Global electricity demand, generation, grid system, and renewable energy policies: a review. *Wiley Interdiscip. Rev. Energy Environ.* **6**, e222 (2017).
- United Nations Educational, Scientific and Cultural Organization (UNESCO). World Water Assessment Programme. *The United Nations World Water Development Report: Valuing Water* (UNESCO Publishing, Paris, France, 2021).
- Burek, P. et al. *Water Futures And Solution-Fast Track Initiative*. <https://pure.iiasa.ac.at/id/eprint/13008/> (2016).
- United Nations, Department of Economic and Social Affairs, Population Division (UN DESA). *World Population Prospects: The 2015 Revision, Key Findings And Advance Tables*. https://population.un.org/wpp/Publications/Files/Key_Findings_WPP_2015.pdf (2015).
- Kramer, I., Tsairi, Y., Roth, M. B., Tal, A. & Mau, Y. Effects of population growth on Israel's demand for desalinated water. *npj Clean. Water* **5**, 1–7 (2022).
- Boretti, A. & Rosa, L. Reassessing the projections of the world water development report. *npj Clean. Water* **2**, 1–6 (2019).
- Milan, B. F. Clean water and sanitation for all: interactions with other sustainable development goals. *Sustain. Water Resour. Manag.* **3**, 479–489 (2017).
- Haque, S. et al. Effects of adding household water filters to rwanda's community-based environmental health promotion programme: a cluster-randomized controlled trial in rwamagana district. *npj Clean. Water* **5**, 42 (2022).
- Ozturk, I., Aslan, A. & Kalyoncu, H. Energy consumption and economic growth relationship: evidence from panel data for low and middle income countries. *Energy Policy* **38**, 4422–4428 (2010).
- IEA. *Electricity Demand And Real GDP Growth In Emerging And Developing Economies, 1990–2021*. <https://www.iea.org/data-and-statistics/charts/electricity-demand-and-real-gdp-growth-in-emerging-and-developing-economies-1990-2021> (2020).
- Food and Agriculture Organization of the United Nations (FAO). *AQUASTAT Database*. <http://www.fao.org/aquastat/statistics/query/index.html> (2021).
- Sharma, R. K., Yadav, M. & Gupta, R. Chapter five—water quality and sustainability in India: challenges and opportunities. *Chem. Water* <https://doi.org/10.1016/B978-0-12-809330-6.00005-2> (2017).
- Berners-Lee, M. *How Bad Are Bananas?: The Carbon Footprint Of Everything* Main edition, 304 (Profile Books, 2020).
- Ghaffour, N. & Mujtaba, I. M. Desalination using renewable energy. *Desalination* **435**, 1–2 (2018).
- Liu, J., Chen, S., Wang, H. & Chen, X. Calculation of carbon footprints for water diversion and desalination projects. *Energy Procedia* **75**, 2483–2494 (2015).
- United Nations General Assembly. *Transforming Our World: The 2030 Agenda For Sustainable Development*. <https://sustainabledevelopment.un.org/post2015/transformingourworld/publication> (2015).
- Herrando, M., Markides, C. N. & Hellgardt, K. A UK-based assessment of hybrid PV and solar-thermal systems for domestic heating and power: system performance. *Appl. Energy* **122**, 288–309 (2014).
- Chandrasekar, M. & Senthilkumar, T. Five decades of evolution of solar photovoltaic thermal (PVT) technology – a critical insight on review articles. *J. Clean. Prod.* **322**, 128997 (2021).
- Skoplaki, E. & Palyvos, J. A. On the temperature dependence of photovoltaic module electrical performance: a review of efficiency/power correlations. *Sol. Energy* **83**, 614–624 (2009).
- Ebrahimi, M., Aramesh, M. & Khanjari, Y. Innovative ANP model to prioritize of PV/T systems based on cost and efficiency approaches: with a case study for Asia. *Renew. Energy* **117**, 434–446 (2018).
- Pathak, M. J. M., Sanders, P. G. & Pearce, J. M. Optimizing limited solar roof access by exergy analysis of solar thermal, photovoltaic, and hybrid photovoltaic thermal systems. *Appl. Energy* **120**, 115–124 (2014).
- Herrando, M. et al. A review of solar hybrid photovoltaic-thermal (PV-T) collectors and systems. *Prog. Energy Combust. Sci.* **97**, 101072 (2023).
- Esmailion, F. Hybrid renewable energy systems for desalination. *Appl. Water Sci.* **10**, 84 (2020).
- González, D., Amigo, J. & Suárez, F. Membrane distillation: perspectives for sustainable and improved desalination. *Renew. Sustain. Energy Rev.* **80**, 238–259 (2017).
- Khraisheh, M., Benyahia, F. & Adham, S. Industrial case studies in the petrochemical and gas industry in qatar for the utilization of industrial waste heat for the production of fresh water by membrane desalination. *Desalin. Water Treat.* **51**, 1769–1775 (2013).
- Zhang, L. et al. Passive, high-efficiency thermally-localized solar desalination. *Energy Environ. Sci.* **14**, 1771–1793 (2021).
- Jones, E., Qadir, M., van Vliet, M. T. H., Smakhtin, V. & Kang, S.-M. The state of desalination and brine production: a global outlook. *Sci. Total Environ.* **657**, 1343–1356 (2019).
- López-Porfiri, P., Ramos-Paredes, S., Núñez, P. & Gorgojo, P. Towards the technological maturity of membrane distillation: the MD module performance curve. *npj Clean. Water* **6**, 1–9 (2023).
- Al-Mutaz, I. & Ghunaimi, M. *Performance of Reverse Osmosis Units At High Temperatures*. <https://ida.memberclicks.net/assets/docs/1099.1.pdf> (2001).
- Koutsou, C. P., Kritikos, E., Karabelas, A. J. & Kostoglou, M. Analysis of temperature effects on the specific energy consumption in reverse osmosis desalination processes. *Desalination* **476**, 114213 (2020).

36. Abdelkareem, M. A., El Haj Assad, M., Sayed, E. T. & Soudan, B. Recent progress in the use of renewable energy sources to power water desalination plants. *Desalination* **435**, 97–113 (2018).
37. United Nations General Assembly. Res. 64/292. *The Human Right To Water And Sanitation*. <https://digitallibrary.un.org/record/687002?ln=en&v=pdf> (2010).
38. Castro, M., Alcanzare, M., Esparcia, E. & Ocon, J. A comparative techno-economic analysis of different desalination technologies in off-grid islands. *Energies* **13**, 2261 (2020).
39. Ghenai, C., Kabakebji, D., Douba, I. & Yassin, A. Performance analysis and optimization of hybrid multi-effect distillation adsorption desalination system powered with solar thermal energy for high salinity sea water. *Energy* **215**, 119212 (2021).
40. Quteishat, K. & Abu-Arabi, M. *Promotion Of Solar Desalination In The MENA Region*. https://sswm.info/sites/default/files/reference_attachments/QUTEISHAT%20and%20ABU-ARABI%202004%20Promotion%20of%20Solar%20Desalination%20in%20the%20MENA%20Region.pdf (2006).
41. Al-Karaghoul, A. & Kazmerski, L. L. Energy consumption and water production cost of conventional and renewable-energy-powered desalination processes. *Renew. Sustain. Energy Rev.* **24**, 343–356 (2013).
42. Mezher, T., Fath, H., Abbas, Z. & Khaled, A. Techno-economic assessment and environmental impacts of desalination technologies. *Desalination* **266**, 263–273 (2011).
43. Morin, O. J. Design and operating comparison of MSF and MED systems. *Desalination* **93**, 69–109 (1993).
44. Shahzad, M. W., Thu, K., Kim, Y.-D. & Ng, K. C. An experimental investigation on MEDAD hybrid desalination cycle. *Appl. Energy* **148**, 273–281 (2015).
45. Falk, J., Globisch, B., Angelmahr, M., Schade, W. & Schenk-Mathes, H. Drinking water supply in rural africa based on a Mini-Grid energy system—A socio-economic case study for rural development. *Sustain. Sci. Pract. Policy* **14**, 9458 (2022).
46. Sayani, R. et al. Sizing solar-based mini-grids for growing electricity demand: insights from rural India. *J. Phys. Energy* **5**, 014004 (2022).
47. Zhang, Z. et al. Theoretical analysis of a solar-powered multi-effect distillation integrated with concentrating photovoltaic/thermal system. *Desalination* **468**, 114074 (2019).
48. Giwa, A., Yusuf, A., Dindi, A. & Balogun, H. A. Polygeneration in desalination by photovoltaic thermal systems: a comprehensive review. *Renew. Sustain. Energy Rev.* **130**, 109946 (2020).
49. Ammous, M. & Chaabene, M. Design of a PV/T based desalination plant: Concept and assessment. In *5th International Renewable Energy Congress (IREC)* <https://doi.org/10.1109/IREC.2014.6827025> (IREC, 2014).
50. Sandwell, P., Winchester, B., Beath, H. & Nelson, J. CLOVER: A modelling framework for sustainable community-scale energy systems. *J. Open Source Softw.* **8**, 4799 (2023).
51. Winchester, B., Beath, H., Nelson, J. & Sandwell, P. CLOVER: A modelling framework for sustainable community-scale energy systems. *Zenodo* <https://doi.org/10.5281/zenodo.6925534> (2023).
52. Givler, T. & Lillenthal, P. *Using HOMER software, NREL's Micropower Optimization Model, to Explore the Role of Gen-sets in Small Solar Power Systems; Case Study: Sri Lanka*. <https://www.nrel.gov/docs/fy05osti/36774.pdf> (2005).
53. Dufo-López, R. *iHOGA / MHOGA—Simulation and Optimization of Stand-Alone and Grid-Connected Hybrid Renewable Systems*. <https://ihoga.unizar.es/en/> (2013).
54. Qiblawey, Y., Alassi, A., Zain ul Abideen, M. & Bañales, S. Techno-economic assessment of increasing the renewable energy supply in the canary islands: the case of tenerife and gran canaria. *Energy Policy* **162**, 112791 (2022).
55. Joo, H.-J. & Kwak, H.-Y. Performance evaluation of multi-effect distiller for optimized solar thermal desalination. *Appl. Therm. Eng.* **61**, 491–499 (2013).
56. Elsaid, K. et al. Environmental impact of desalination technologies: a review. *Sci. Total Environ.* **748**, 141528 (2020).
57. El-Nashar, A. M. & Samad, M. The solar desalination plant in abu Dhabi: 13 years of performance and operation history. *Renew. Energy* **14**, 263–274 (1998).
58. Rahimi, B., May, J., Christ, A., Regenauer-Lieb, K. & Chua, H. T. Thermo-economic analysis of two novel low grade sensible heat driven desalination processes. *Desalination* **365**, 316–328 (2015).
59. Zhang, Y., Sivakumar, M., Yang, S., Enever, K. & Ramezani-pour, M. Application of solar energy in water treatment processes: a review. *Desalination* **428**, 116–145 (2018).
60. Zheng, Y., Caceres Gonzalez, R. A., Hatzell, K. B. & Hatzell, M. C. Large-scale solar-thermal desalination. *Joule* **5**, 1971–1986 (2021).
61. Baniasad Askari, I. & Ameri, M. A techno-economic review of multi effect desalination systems integrated with different solar thermal sources. *Appl. Therm. Eng.* **185**, 116323 (2021).
62. Gangar, N., Macchietto, S. & Markides, C. N. Recovery and utilization of low-grade waste heat in the oil-refining industry using heat engines and heat pumps: an international technoeconomic comparison. *Energies* **13**, 2560 (2020).
63. Milosavljević, D. D., Kevkić, T. S. & Jovanović, S. J. Review and validation of photovoltaic solar simulation tools/software based on case study. *Open Phys.* **20**, 431–451 (2022).
64. Christ, A., Regenauer-Lieb, K. & Chua, H. T. Thermodynamic optimisation of multi effect distillation driven by sensible heat sources. *Desalination* **336**, 160–167 (2014).
65. Fraunhofer Institute for Solar Energy Systems & ISE with support of PSE Projects GmbH. *Photovoltaics Report*. <https://www.ise.fraunhofer.de/content/dam/ise/de/documents/publications/studies/Photovoltaics-Report.pdf> (2022).
66. Spotnitz, R. Simulation of capacity fade in lithium-ion batteries. *J. Power Sources* **113**, 72–80 (2003).
67. Yang, X.-G., Zhang, G., Ge, S. & Wang, C.-Y. Fast charging of lithium-ion batteries at all temperatures. *Proc. Natl Acad. Sci. USA* **115**, 7266–7271 (2018).
68. Rohr, S. et al. Quantifying uncertainties in reusing lithium-ion batteries from electric vehicles. *Procedia Manuf.* **8**, 603–610 (2017).
69. Peng, X., Chen, S., Garg, A., Bao, N. & Panda, B. A review of the estimation and heating methods for lithium-ion batteries pack at the cold environment. *Energy Sci. Eng.* **7**, 645–662 (2019).
70. Sangwongwanich, A., Yang, Y., Sera, D. & Blaabjerg, F. Lifetime evaluation of grid-connected PV inverters considering panel degradation rates and installation sites. *IEEE Trans. Power Electron.* **PP**, 1–10 (2017).
71. Anis, S. F., Hashaikh, R. & Hilal, N. Reverse osmosis pretreatment technologies and future trends: a comprehensive review. *Desalination* **452**, 159–195 (2019).
72. Dias Xavier, L., Yokoyama, L., Reich de Oliveira, V., Travagini Ribeiro, G. & Araujo, O. The role of coagulation-flocculation in the pretreatment of reverse osmosis in power plant. *J. Sustain. Dev. Energy Water Environ. Syst.* **8**, 118–131 (2020).
73. Djebedjian, B., Gad, H., Adou Rayan, M. M. & Khaled, I. Experimental and analytical study of a reverse osmosis desalination plant (dept.m). *Mansoura Eng. J.* **34**, 71–92 (2020).
74. Olympos, A. V., Mersch, M., Sapin, P., Pantaleo, A. M. & Markides, C. N. Library of price and performance data of domestic and commercial technologies for low-carbon energy systems. *Zenodo* <https://doi.org/10.5281/ZENODO.4692648> (2021).
75. Hong, W. et al. Recent progress in thermal energy recovery from the decoupled photovoltaic/thermal system equipped with spectral splitters. *Renew. Sustain. Energy Rev.* **167**, 112824 (2022).
76. Kim, J. et al. A review of the degradation of photovoltaic modules for life expectancy. *Energies* **14**, 4278 (2021).
77. Huang, G. & Markides, C. N. Spectral-splitting hybrid PV-thermal (PV-T) solar collectors employing semi-transparent solar cells as optical filters. *Energy Convers. Manag.* **248**, 114776 (2021).

78. Guarracino, I., Mellor, A., Ekins-Daukes, N. J. & Markides, C. N. Dynamic coupled thermal-and-electrical modelling of sheet-and-tube hybrid photovoltaic/thermal (PVT) collectors. *Appl. Therm. Eng.* **101**, 778–795 (2016).
79. Ma, T., Li, M. & Kazemian, A. Photovoltaic thermal module and solar thermal collector connected in series to produce electricity and high-grade heat simultaneously. *Appl. Energy* **261**, 114380 (2020).
80. Bobanac, V., Bašić, H. & Pandžić, H. Determining lithium-ion battery one-way energy efficiencies: Influence of c-rate and coulombic losses. In *19th International Conference on Smart Technologies* <https://doi.org/10.1109/EUROCON52738.2021.9535542> (IEEE, 2021).
81. Preger, Y. et al. Degradation of commercial lithium-ion cells as a function of chemistry and cycling conditions. *J. Electrochem. Soc.* **167**, 120532 (2020).
82. Huld, T., Müller, R. & Gambardella, A. A new solar radiation database for estimating PV performance in Europe and Africa. *Sol. Energy* **86**, 1803–1815 (2012).
83. Quansah, D. A., Adaramola, M. S. & Takyi, G. Degradation and longevity of solar photovoltaic modules—an analysis of recent field studies in Ghana. *Energy Sci. Eng.* **8**, 2116–2128 (2020).
84. Cabello, V. et al. *MAGIC Moving Towards Adaptive Governance In Complexity: Informing Nexus sSecurity GA no. 689669, Funding Type RIA Deliverable Number (relative in WP)*. <https://research.wur.nl/en/publications/magic-moving-towards-adaptive-governance-in-complexity-informing-> (2020).
85. Ortega-Gaucin, D., De la Cruz Bartolón, J. & Castellano Bahena, H. V. Drought vulnerability indices in Mexico. *Water* **10**, 1671 (2018).
86. Arreguin-Cortes, F. I. et al. Municipal level water security indices in Mexico. *SN Appl. Sci.* **1**, 1194 (2019).
87. Arreguin-Cortes, F. I. et al. State level water security indices in Mexico. *Sustain. Earth* **3**, 1–14 (2020).
88. McEvoy, J. Desalination and water security: The promise and perils of a technological fix to the water crisis in Baja California Sur, Mexico. *Water Alternatives* **7**, 518–541 (2014).
89. Friedlingstein, P. et al. Global carbon budget 2022. *Earth Syst. Sci. Data* **14**, 4811–4900 (2022).
90. Santamarta, J. C., Rubiales, I. C., Rodríguez-Martín, J. & Cruz-Pérez, N. Water status in the canary islands related to energy requirements. *Energ. Effic.* **15**, 13 (2022).
91. Barone, G., Buonomano, A., Forzano, C., Giuzio, G. F. & Palombo, A. Supporting the sustainable energy transition in the canary islands: simulation and optimization of multiple energy system layouts and economic scenarios. *Front. Sustain. Cities* **3**, 685525 (2021).
92. Padrón, I., Avila, D., Marichal, G. N. & Rodríguez, J. A. Assessment of hybrid renewable energy systems to supplied energy to autonomous desalination systems in two islands of the canary archipelago. *Renew. Sustain. Energy Rev.* **101**, 221–230 (2019).
93. Department for Energy Security and Net Zero & Department for Business, Energy and Industrial Strategy. *Historical Electricity Data*. <https://www.gov.uk/government/statistical-data-sets/historical-electricity-data> (2022).
94. Kolb, S., Dillig, M., Plankenbühler, T. & Karl, J. The impact of renewables on electricity prices in Germany - an update for the years 2014–2018. *Renew. Sustain. Energy Rev.* **134**, 110307 (2020).
95. Nelder, J. A. & Mead, R. A simplex method for function minimization. *Comput. J.* **7**, 308–313 (1965).
96. Liu, D. C. & Nocedal, J. On the limited memory BFGS method for large scale optimization. *Math. Program.* **45**, 503–528 (1989).
97. Diouf, B. & Podes, R. Potential of lithium-ion batteries in renewable energy. *Renew. Energy* **76**, 375–380 (2015).
98. Gangwar, T., Padhy, N. P. & Jena, P. Storage allocation in active distribution networks considering life cycle and uncertainty. *IEEE Trans. Ind. Inf.* **19**, 339–350 (2023).
99. Ghaithan, A. M., Mohammed, A. & Hadidi, L. Assessment of integrating solar energy with reverse osmosis desalination. *Sustain. Energy Technol. Assess.* **53**, 102740 (2022).
100. Caldera, U., Bogdanov, D. & Breyer, C. in *Energy Powered Desalination Handbook* Ch. 8 (Elsevier Inc., 2018).
101. Shahabi, M. P., McHugh, A., Anda, M. & Ho, G. Environmental life cycle assessment of seawater reverse osmosis desalination plant powered by renewable energy. *Renew. Energy* **67**, 53–58 (2014).
102. International Renewable Energy Agency. *Renewable Power Generation Costs In 2021* <https://www.irena.org/publications/2022/Jul/Renewable-Power-Generation-Costs-in-2021> (2022).
103. Ziegler, M. S. & Trancik, J. E. Re-examining rates of lithium-ion battery technology improvement and cost decline. *Energy Environ. Sci.* **14**, 1635–1651 (2021).

Acknowledgements

This work was supported by the UK Engineering and Physical Sciences Research Council (EPSRC) [grant numbers EP/R045518/1, and EP/X52556X/1] and the UK Natural Environment Research Council (NERC) [grant numbers NE/S007415/1, and NE/R011613/1]. The work was also supported by the Royal Society under an International Collaboration Award 2020 [grant number ICA\R1\201302]. B.W. and H.B. would like to gratefully acknowledge the support of NERC and the Grantham Institute - Climate Change and the Environment for Ph.D. scholarships. J.N. thanks the Royal Society for the award of a Research Professorship and the European Research Council for award of an Advanced Grant (grant number 742708, CAPaCITY). The authors would like to thank Dr Andreas Olympios for guidance surrounding heat-pump modelling techniques and associated embedded emissions, Paloma Ortega-Arriaga for her help translating the website of the Comisión Federal de Electricidad, and Matthias Mersch for his help determining the pinch-point temperature difference to use for the heat pumps modelled. The authors would also like to thank UK company Solar Flow Ltd. (<http://www.solar-flow.co.uk>) and Dutch company Desolenator B.V. (<https://www.desolenator.com>). Data supporting this publication can be obtained on request from cep-lab@imperial.ac.uk and from Zenodo via <https://doi.org/10.5281/zenodo.7801893> with open-source methodology and available at <https://github.com/BenWinchester/HEATDesalination>.

Author contributions

The manuscript was written with the contributions of all authors. All authors have given approval for the final version of the manuscript. B.W., G.H., P.S., J.C., J.N. and C.N.M. conceived of the presented study. B.W., G.H. and P.S. contributed to the design of the software used in the study. B.W. wrote the software used in, and carried out, the computations. J.N. and C.N.M. supervised the project and motivated the selection of case-study technologies and locations considered. B.W. and H.B. planned the investigations surrounding sensitivity to component degradation and the associated emissions. B.W. carried out the emissions analysis, and B.W., H.B., and J.N. analysed the outputs. All authors discussed the results and contributed to the final manuscript.

Competing interests

The authors declare no competing interests.

Additional information

Supplementary information The online version contains supplementary material available at <https://doi.org/10.1038/s41545-024-00335-4>.

Correspondence and requests for materials should be addressed to Christos N. Markides.

Reprints and permissions information is available at <http://www.nature.com/reprints>

Publisher's note Springer Nature remains neutral with regard to jurisdictional claims in published maps and institutional affiliations.

Open Access This article is licensed under a Creative Commons Attribution 4.0 International License, which permits use, sharing, adaptation, distribution and reproduction in any medium or format, as long as you give appropriate credit to the original author(s) and the source, provide a link to the Creative Commons licence, and indicate if changes were made. The images or other third party material in this article are included in the article's Creative Commons licence, unless indicated otherwise in a credit line to the material. If material is not included in the article's Creative Commons licence and your intended use is not permitted by statutory regulation or exceeds the permitted use, you will need to obtain permission directly from the copyright holder. To view a copy of this licence, visit <http://creativecommons.org/licenses/by/4.0/>.

© The Author(s) 2024